Buz A. McCain
e-mail: bmccain@umich.edu

Anna G. Stefanopoulou
e-mail: annastef@umich.edu

Department of Mechanical Engineering,
Fuel Cell Control Laboratory,
University of Michigan,
Ann Arbor, MI 48109

Jason B. Siegel
Department of Electrical Engineering Systems,
Fuel Cell Control Laboratory,
University of Michigan,
Ann Arbor, MI 48109
e-mail: siegeljb@umich.edu

Controllability and Observability Analysis of the Liquid Water Distribution Inside the Gas Diffusion Layer of a Unit Fuel Cell Model

We analyze the controllability and observability (C/O) of the liquid water distribution in the gas diffusion layer (GDL) of a polymer electrolyte membrane fuel cell (PEMFC) using a one-dimensional channel-to-channel unit fuel cell model. This modeling domain is sufficient to illustrate the control objectives and analysis techniques but requires further development for stack level modeling. A comparison is made between first-principles-based numeric and reduced-order semi-analytic models with emphasis on the effects of model reduction on their analyses. The numeric model is a partial differential equation based model approximated by difference equations, including both channels and both GDLs of a PEMFC. The reduced model uses a semi-analytic solution method, which is a combination of analytic and numeric solutions, gaining physical intuition at lower computational cost. The C/O analysis is based on linearizations around three critical operating points. The results indicate that stabilizability of the anode liquid water states and, hence, management of anode water flooding is possible. If the channel water mass can be controlled to a constant value, then the GDL liquid distribution will be stable (McCain et al., 2007, "A Multi-Component Spatially-Distributed Model of Two-Phase Flow for Estimation and Control of Fuel Cell Water Dynamics," Proceedings of the 46th IEEE Conference on Decision and Control, pp. 584–589). Further, it will be shown that if the channel liquid water mass can be brought to zero, controllability of the GDL liquid modes will be obtained. Additionally, this study will indicate the input(s) best suited to obtain this control objective and the output(s) required. [DOI: 10.1115/1.4002477]

1 Introduction and Motivation

The quantity of water within each region of a polymer electrolyte membrane fuel cell (PEMFC) directly affects the system performance, efficiency, and durability. High membrane humidity is desirable for proton conductivity, yet excess liquid water in the cathode catalyst layer (at high current density) and in the gas channels have been experimentally shown to be a cause of output voltage degradation [1–3]. Although critical for extending high power operation, cathode catalyst flooding is typically treated as a materials design problem [4] rather than a subject for active control, as opposed to channel flooding, where the gas flow rate and inlet relative humidity can be effectively applied as actuators. Due to the low gas velocity in the anode channel, liquid water removal from this volume is more difficult than the cathode [5]. The anode water management issue is also very important because of the cost, weight, and system packaging requirements (component size) of anode systems, where hydrogen grade plumbing is required. However, the techniques outlined in this paper are not unique to the anode side liquid distribution, and one could perform the same analysis for the cathode.

Liquid water exiting the gas diffusion layer (GDL) and accumulating in the anode channel impedes the ability of hydrogen to enter the GDL and reach the membrane, ultimately reducing the fuel cell active area [6] and causing a decrease in cell voltage, which is however recoverable. Removal of accumulated liquid water is necessary to regain performance and is typically accomplished by intermittently increasing an inlet flow (e.g., anode H_2 supply). While it is generally understood that hydrophobicity of the GDL porous media facilitates the liquid transport from GDL to channel and the accumulation of water in the channel effects, the GDL liquid water distribution [1,2,5], the interaction between GDL and channel liquid water has yet to be addressed from a controls perspective. This is a critical step for the establishment of algorithms to control liquid water within the fuel cell.

The use of a one-dimensional (1D) channel-to-channel unit fuel cell model illustrates the control objectives and analysis techniques. Extension of the unit cell model to along the channel dimension is the subject of ongoing research, so that the C/O analysis can be applied to interpret the effects of spatial variations occurring along the channel in large stacks.

The model from Ref. [7] describing the multicomponent (reactants and water), two-phase (vapor and liquid water), spatially-distributed, dynamic behavior across the GDL (Fig. 1) is employed to study controllability/observability (C/O) for fuel cell water management. The time-varying constituent distributions in the GDL of each electrode are described by three second-order parabolic partial differential equations (PDEs) for reactant (oxygen in the cathode and hydrogen in the anode) concentration, water vapor concentration, and liquid water volume. The electrochemical reactions on, and the mass transport through, the catalyst-covered membrane couple the anode and cathode behaviors and, together with the channel conditions, provide the time-varying boundary values for these PDEs.

A C/O analysis based on linearization around different operating points shows that it is mathematically possible to control the

---

Contributed by the Dynamic Systems Division of ASME for publication in the Journal of Dynamic Systems, Measurement, and Control. Manuscript received September 30, 2008; final manuscript received July 28, 2010; published online October 29, 2010. Assoc. Editor: Loucas Louca.

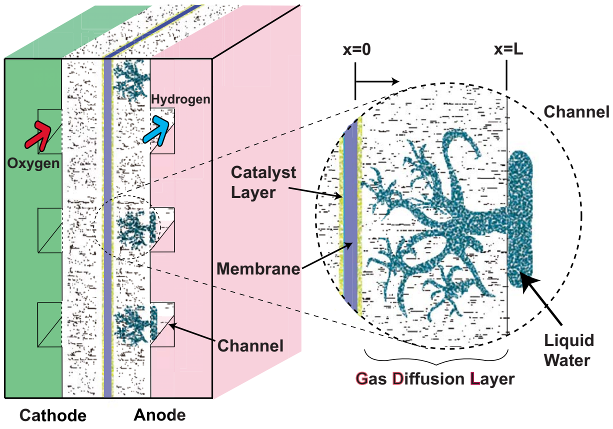

Fig. 1 Conceptual schematic showing accumulation of liquid water in the GDL and subsequent flow to the channel to form reactant-blocking film

GDL-channel boundary conditions (BC), which is critical for the stabilization of the liquid water states in the fuel cell channels. It is demonstrated that the C/O is affected by the operating point. For example, greater controllability of the liquid water modes is obtained when the channel condition is subsaturated than when it is saturated. On the other hand, during anode channel flooding (which is associated with channel vapor saturation), the GDL anode liquid water becomes uncontrollable, yet observability is gained using cell voltage output.

2 Fuel Cell Model

A summary of the first principles model for the anode will be provided here. The details of the model are identical to those presented in Ref. [7] and validation of the model can be found in Ref. [8].

We proceed with a one-dimensional treatment focusing on the anode, using the following assumptions.

1. The model is spatially isothermal.
2. Convective flow of the gases in the GDL is neglected.
3. Mass transport is in 1-D, normal to the membrane.
4. Water transport out of the anode channel is in vapor form.
5. A uniform current density exists across the unit cell.

We designate x as the spatial variable, with $x=0$ corresponding to the membrane location and $x=L$ corresponding to the anode channel location as shown in Fig. 1, and we let t denote time.

The state variables are as follows.

1. $c_{\rm H_2}(x,t)$ is the hydrogen concentration $({\rm mol/m^3})$ at time t at a cross-section of the GDL located at x, $0 \leq x \leq L$.
2. $c_{v,{\rm an}}(x,t)$ is the concentration of water vapor at time t at a cross-section of GDL located at x, $0 \leq x \leq L$.
3. The liquid saturation $s(x,t)$ is the fraction of liquid water volume V_L to the total pore volume V_p, $s=V_L/V_p$. s is thus a concentration-like variable for the liquid water at time t, at a cross-section of GDL located at x, $0 \leq x \leq L$.

Also taken from Ref. [9] and simplified in Ref. [7], the molar fluxes are driven entirely by the presence of a concentration gradient (i.e., diffusion) since bulk flow (convection) is neglected,

$$N_{\rm H_2} = -D_{\rm H_2}(s)\frac{\partial c_{\rm H_2}}{\partial x}, \quad N_v = -D_v(s)\frac{\partial c_{v,{\rm an}}}{\partial x} \tag{1}$$

where $D_v(s)$ and $D_{\rm H_2}(s)$ are the effective diffusivity for water vapor and hydrogen, which depend on the water saturation s,

$$D_j(s) = D_{\varepsilon,j}(1-s)^2 \approx D_{\varepsilon,j}(1-s_{\rm im})^2 \triangleq D_v^{s_{\rm im}} \tag{2}$$

where $D_{\varepsilon,j}$ is a constant that depends on GDL porosity (ε).

2.1 Gas Diffusion Layer Model.

The gas concentrations are

$$\frac{\partial c_{\rm H_2}}{\partial t} = -\frac{\partial N_{\rm H_2}}{\partial x}, \quad \frac{\partial c_{v,{\rm an}}}{\partial t} = -\frac{\partial N_v}{\partial x} + r_v(c_{v,{\rm an}}) \tag{3}$$

where r_v is the evaporation rate defined as

$$r_v(c_{v,{\rm an}}) = \begin{cases} \gamma(c_v^{\rm sat} - c_{v,{\rm an}}) & \text{for } s > 0, \\ \min\{0, \gamma(c_v^{\rm sat} - c_{v,{\rm an}})\} & \text{for } s = 0 \end{cases}$$

The water (liquid and vapor) PDEs are coupled through this evaporation/condensation rate, where γ is the volumetric condensation coefficient and $c_v^{\rm sat}$ is the vapor saturation concentration. Note that evaporation can only occur if there is liquid water ($s > 0$) in the GDL.

Conservation of liquid mass is employed to determine the rate of liquid accumulation

$$\frac{\partial s}{\partial t} = -\frac{1}{\varepsilon A_{\rm fc}\rho_l}\frac{\partial W_l}{\partial x} - \frac{M_v}{\rho_l}r_v(c_{v,{\rm an}}) \tag{4}$$

where M_v is the vapor molar mass, $A_{\rm fc}$ $({\rm m^2})$ is the fuel cell active area, and ρ_l $({\rm kg/m^3})$ is the density of liquid water.

The mass flow of liquid water ($W_l(x,t)$ $({\rm kg/s})$) is driven by the capillary pressure (p_c) gradient due to accumulation of liquid water in the GDL,

$$W_l = -\varepsilon A_{\rm fc}\rho\frac{KK_{\rm rl}}{\mu_l}\frac{\partial p_c}{\partial x} \tag{5}$$

where μ_l (kg/ms) is the liquid viscosity and K is the material-dependent absolute permeability $({\rm m^2})$, where the relative liquid permeability is $K_{\rm rl}=S^3$. The reduced liquid saturation $S(x,t)$ is

$$S(x,t) \triangleq \begin{cases} \dfrac{s(x,t) - s_{\rm im}}{1 - s_{\rm im}} & \text{for } s(x,t) \geq s_{\rm im} \\ 0 & \text{for } s(x,t) < s_{\rm im} \end{cases} \tag{6}$$

with $s_{\rm im}=0.1$ from Ref. [9]. The condensed liquid accumulates in the GDL until the liquid water ratio surpasses the immobile saturation ($s_{\rm im}$), at which point capillary flow will carry it to an area of lower capillary pressure (toward the GDL-channel interface).

We assume here that the capillary pressure p_c (Pa) is a fitted third-order polynomial in $S(x,t)$, the liquid water saturation

$$p_c = \beta_{pc}(1.417S - 2.12S^2 + 1.263S^3) \tag{7}$$

where β_{pc} is a function of surface tension, absolute permeability, viscosity, and porosity [9]. The use of another capillary pressure model to account for different material properties, such as the one presented in Ref. [10], is also possible within this framework and would not affect the resulting C/O analysis but only the model predicted equilibrium values.

To facilitate analysis, Eq. (5) is rewritten as

$$W_l = -\varepsilon A_{\rm fc}\rho_l\frac{K}{\mu_l}S^3\frac{dp_c}{dS}\frac{dS}{dx} \approx -\varepsilon A_{\rm fc}\rho_l b_1 S^{b_2}\frac{dS}{dx} \tag{8}$$

using an approximation $(K/\mu_l)S^3(dp_c/dS) \approx b_1 S^{b_2}$, where b_1 and b_2 are fitted parameters.

Combining Eq. (1) with Eq. (3) provides the two second-order parabolic PDEs that govern the anode reactant and water vapor concentrations

$$\frac{\partial c_{\rm H_2}}{\partial t} = \frac{\partial}{\partial x}\left(D_{\rm H_2}^{s_{\rm im}}\frac{\partial c_{\rm H_2}}{\partial x}\right) \tag{9}$$

and

$$\frac{\partial c_{v,\mathrm{an}}}{\partial t} = \frac{\partial}{\partial x}\left(D_v^{s_{\mathrm{im}}}\frac{\partial c_{v,\mathrm{an}}}{\partial x}\right) + r_v(c_{v,\mathrm{an}}) \tag{10}$$

A similar result is found from Eqs. (4) and (8) s

$$\frac{\partial s}{\partial t} = \frac{\partial}{\partial x}\left(b_1 S^{b_2}\frac{\partial S}{\partial x}\right) - \frac{M_v}{\rho_l} r_v(c_{v,\mathrm{an}}) \tag{11}$$

2.2 Boundary Conditions. For $c_{\mathrm{H}_2}(x,t)$, mixed Neumann–Dirichlet type boundary conditions are imposed. The channel (ch) BC is

$$c_{\mathrm{H}_2}|_{x=L} = c_{\mathrm{H}_2}^{\mathrm{ch}} = p_{\mathrm{H}_2}^{\mathrm{ch}}/(\mathcal{R}T) \tag{12}$$

where $\mathcal{R}$ is the universal gas constant, T is the temperature, and the anode channel hydrogen partial pressure $p_{\mathrm{H}_2}^{\mathrm{ch}}$ depends on the control $\bar{u}$ as discussed in Sec. 2.3. The membrane (mb) BC is

$$\left.\frac{\partial c_{\mathrm{H}_2}}{\partial x}\right|_{x=0} = -\frac{N_{\mathrm{H}_2}^{\mathrm{rct}}}{D_{\mathrm{H}_2}^{s_{\mathrm{im}}}|_{x=0}} = -\frac{1}{D_{\mathrm{H}_2}^{s_{\mathrm{im}}}|_{x=0}}\cdot\frac{i(t)}{2F} \tag{13}$$

where rct indicates the reaction of H_2 at the anode catalyst, which depends on current density i, and F is Faraday's constant.

For $c_{v,e}(x,t)$, similar mixed BC are imposed $(e=\mathrm{an},\mathrm{ca})$

$$c_{v,e}|_{x=\pm L} = c_{v,e}^{\mathrm{ch}} = p_{v,e}^{\mathrm{ch}}/(\mathcal{R}T) \tag{14}$$

$$\left.\frac{\partial c_{v,\mathrm{an}}}{\partial x}\right|_{x=0} = \frac{-N^{\mathrm{mb}}}{D_v^{s_{\mathrm{im}}}}, \qquad \left.\frac{\partial c_{v,\mathrm{ca}}}{\partial x}\right|_{x=0} = \frac{N_v^{\mathrm{rct}} - N^{\mathrm{mb}}}{D_v^{s_{\mathrm{im}}}} \tag{15}$$

where $N_v^{\mathrm{rct}}=i/(2F)$ is from the formation of $\mathrm{H_2O}$ at the cathode catalyst and the membrane water molar flux N^{mb} is governed by electro-osmotic drag and back diffusion

$$N^{\mathrm{mb}} = n_d\frac{i}{F} - D_w\frac{(c_{v,\mathrm{ca}}|_{x=0} - c_{v,\mathrm{an}}|_{x=0})}{t_{\mathrm{mb}}} \tag{16}$$

which are driven by current density and the gradient in $c_{v,e}$ across the membrane, respectively. t_{mb} is the membrane thickness. The electro-osmotic drag coefficient n_d and the membrane water vapor diffusion coefficient D_w both depend on the membrane water content, which is calculated from the average water activity on each side of the membrane as described in Ref. [6]. Although more complex models could be used that include liquid water transport and liquid pressure, we consider conditions for which there is little or no pressure difference across the membrane.

Finally, for the liquid water PDE, mixed BC are again imposed. Specifically, since water passing into the GDL from the membrane is in vapor form due to the assumed presence of a microporous barrier layer

$$\left.\frac{\partial S}{\partial x}\right|_{x=0} = 0 \tag{17}$$

The liquid water boundary condition at the GDL-channel interface is an issue of ongoing research. A common assumption is that the hydrophobic nature of the GDL porous media essentially pushes the liquid water into the channel (formed of hydrophilic material) with zero resistance [9], or zero capillary pressure [11]. On the other hand, Zhang et al. [2] and Sinha and Wang [12] suggested that the presence of liquid water on the GDL-channel interface constitutes a resistance to flow into the channel. There does not exist yet a physics-based method to relate the amount of liquid water in the channel to resistance to flow from the GDL. In Ref. [13], various values of $s(L,t)$ were selected without stated reason and kept fixed for simulation, and in Ref. [12], a constant capillary back-pressure was assumed (7.7 kPa) without explanation for the choice. Since capillary pressure is determined as a function of the reduced water saturation (Eq. (7)), setting values of $S(L,t)$ is equivalent to setting back capillary pressure.

A general form of the liquid boundary condition at the GDL-channel interface

$$S(L,t) = g(m_{\mathrm{lw}}^{\mathrm{ch}}(t)) \tag{18}$$

as suggested in Ref. [14] accommodates many of the possible physical mechanisms reported in the literature. The only assumption is that g is a monotonic and exponentially bounded function of the mass of liquid water in the channel $m_{\mathrm{lw}}^{\mathrm{ch}}(t)$. A form for g was not proposed because it was shown that control of $m_{\mathrm{lw}}^{\mathrm{ch}}$, and hence a bounded $g(m_{\mathrm{lw}}^{\mathrm{ch}})$, implies stability of the system. As a result, it is assumed that the liquid water at the channel will take a small, nonzero value, thus the channel liquid boundary condition is

$$S(L,t) = s_\delta > 0 \tag{19}$$

Note here that by assuming, $s_\delta > 0$ in Eq. (19), our C/O results will be invariant to the specific functional form of Eq. (18).

2.3 Anode Channel Equations. For the anode channel, the governing equations for hydrogen and water are

$$dm_{\mathrm{H}_2}^{\mathrm{ch}}/dt = W_{\mathrm{H}_2}^{\mathrm{in}} - W_{\mathrm{H}_2}^{\mathrm{out}} + W_{\mathrm{H}_2}^{\mathrm{GDL}}$$

$$dm_w^{\mathrm{ch}}/dt = W_w^{\mathrm{GDL}} - (W_v^{\mathrm{out}} - W_v^{\mathrm{in}}) \tag{20}$$

For generally humidified anode inlet flow with relative humidity ($\mathrm{RH^{in}}$) and prescribed inlet flow rate ($W_{\mathrm{H}_2}^{\mathrm{in}}$) the inlet water mass flow rate is

$$W_v^{\mathrm{in}} = \frac{P_v^{\mathrm{in}}}{P_{\mathrm{H}_2}^{\mathrm{in}}}\frac{M_v}{M_{\mathrm{H}_2}}W_{\mathrm{H}_2}^{\mathrm{in}} \tag{21}$$

where $P_v^{\mathrm{in}}=\mathrm{RH^{in}}P_v^{\mathrm{sat}}$ and $P_{\mathrm{H}_2}^{\mathrm{in}}$ is the pressure of the dry inlet gas.

The H_2 and water vapor partial pressures, which represent the channel-side GDL BC, are calculated from

$$p_{\mathrm{H}_2}^{\mathrm{ch}} = \frac{m_{\mathrm{H}_2}^{\mathrm{ch}}\mathcal{R}T}{M_{\mathrm{H}_2}V_{\mathrm{an}}^{\mathrm{ch}}}$$

$$p_v^{\mathrm{ch}} = \min\left\{\frac{m_w^{\mathrm{ch}}\mathcal{R}T}{M_v V^{\mathrm{ch}}}, p_v^{\mathrm{sat}}\right\}$$

$$p^{\mathrm{ch}} = p_{\mathrm{H}_2}^{\mathrm{ch}} + p_v^{\mathrm{ch}} \tag{22}$$

The liquid water mass in the channel

$$m_{\mathrm{lw}}^{\mathrm{ch}} = m_w^{\mathrm{ch}} - M_v p_v^{\mathrm{ch}} V^{\mathrm{ch}}/(\mathcal{R}T) \tag{23}$$

The anode exit flow rate to the ambient (amb) is modeled as a linearly proportional nozzle equation

$$W^{\mathrm{out}} = \bar{u}\cdot k^{\mathrm{out}}(p^{\mathrm{ch}} - p^{\mathrm{amb}}) \tag{24}$$

where k^{out} is an experimentally determined nozzle orifice constant and $\bar{u}$ is a controllable valve signal $0 \le \bar{u} \le 1$ operating a solenoid valve to remove accumulated channel water and, unfortunately, hydrogen

$$W_{\mathrm{H}_2}^{\mathrm{out}} = \frac{m_{\mathrm{H}_2}^{\mathrm{ch}}}{m^{\mathrm{ch}}}W^{\mathrm{out}}$$

$$W_v^{\mathrm{out}} = W^{\mathrm{out}} - W_{\mathrm{H}_2}^{\mathrm{out}} \tag{25}$$

where $m^{\mathrm{ch}}=m_{\mathrm{H}_2}^{\mathrm{ch}}+p_v^{\mathrm{ch}}V^{\mathrm{ch}}M_v/(\mathcal{R}T)$.

The hydrogen and water mass flow rate from the GDL to the channel are calculated using

$$W_{\mathrm{H}_2}^{\mathrm{GDL}} = -\varepsilon A_{\mathrm{fc}} M_{\mathrm{H}_2}\left.\left(D_{\mathrm{H}_2}^{s_{\mathrm{im}}}\frac{\partial c_{\mathrm{H}_2}}{\partial x}\right)\right|_{x=L}$$

$$W_w^{\mathrm{GDL}} = -\varepsilon A_{\mathrm{fc}}\left(\rho_l b_1 S^{b_2}\frac{\partial S}{\partial x} + M_v D_v^{s_{\mathrm{im}}}\frac{\partial c_v}{\partial x}\right)\Bigg|_{x=L} \tag{26}$$

3 The Semi-Analytic Solutions Model

We pursue model simplification via analytic solution for the purpose of gaining model fidelity without increasing model complexity. By residualizing states using their analytic solution, greater discretization can be accomplished for the states for which closed form solutions have not been found. Higher resolution will reduce the model error and provide more reliable insight into the physics of the system.

The full fuel cell model (both anode and cathode) has 24 states that can be grouped as follows.

- Gas constituents in GDL are 13.
- Liquid constituents in GDL are 6.
- Gas constituents in channels are 5.

Linear time scale decomposition and analysis of the eigenvalues at different channels and GDL water distributions in Ref. [2] indicate that there is a two order of magnitude gap between the minimum gas set eigenvalue and the maximum liquid set eigenvalue for modes within the GDL. The slow mode time constants (liquid) range from 2 s to 25 s, while the fast modes (gas) have time constants ranging 0.32 ms to 0.14 s. This large scale separation indicates that all gas concentrations (including the vapor water concentration) reach equilibrium very fast, and thus the system behavior can be approximated with their steady-state solution when the goal is to control the liquid water accumulation.

3.1 The Water Vapor Solution.

The steady-state solutions implemented for the cathode and anode GDL water vapor distributions are

$$c_{v,\mathrm{an}}(x,t) = \alpha_1 e^{\beta x} + \alpha_2 e^{-\beta x} + c_v^{\mathrm{sat}} \tag{27}$$

$$c_{v,\mathrm{ca}}(x,t) = \nu_1 e^{\beta x} + \nu_2 e^{-\beta x} + c_v^{\mathrm{sat}} \tag{28}$$

where

$$\beta = \sqrt{\gamma / D_v^{s_{im}}} \tag{29}$$

The α_i are functions of the membrane water vapor transport (N^{mb}) and the anode channel condition

$$\alpha_1 e^{\beta L} + \alpha_2 e^{-\beta L} = c_{v,\mathrm{an}}^{\mathrm{ch}} - c_v^{\mathrm{sat}}$$

$$\alpha_1 - \alpha_2 = -N^{\mathrm{mb}}/\beta D_v^{s_{\mathrm{im}}} \tag{30}$$

Determination of N^{mb} given by Eq. (16) requires the knowledge of the water vapor concentrations on both sides of the membrane, which are found from

$$c_{v,\mathrm{an}}^{\mathrm{mb}} = c_{v,\mathrm{an}}|_{x=0} = (\alpha_1 + \alpha_2) + c_v^{\mathrm{sat}}$$

$$c_{v,\mathrm{ca}}^{\mathrm{mb}} = c_{v,\mathrm{ca}}|_{x=0} = (\nu_1 + \nu_2) + c_v^{\mathrm{sat}} \tag{31}$$

where the mb signifies that the value is taken at the membrane ($x=0$). The ν_i, similar to the α_i, is dependent upon N^{mb} and the cathode channel condition but are additionally influenced by the water vapor reaction term N_v^{rct}

$$\nu_1 e^{-\beta L} + \nu_2 e^{\beta L} = c_{v,\mathrm{ca}}^{\mathrm{ch}} - c_v^{\mathrm{sat}}$$

$$\nu_1 - \nu_2 = (-N^{\mathrm{mb}} + N_v^{\mathrm{rct}})/\beta D_v^{s_{\mathrm{im}}} \tag{32}$$

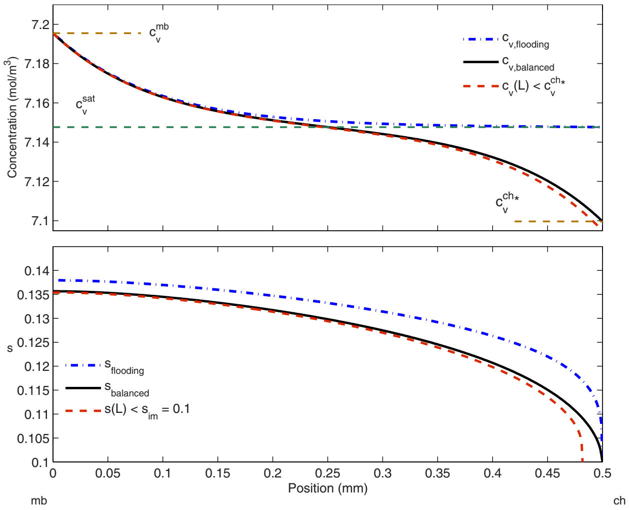

Fig. 2 Anode distribution of liquid water ratio for varying channel water vapor concentrations

3.2 Liquid Water Governing Equation.

An alternate form of the liquid water distribution in the porous medium is obtained by replacing the $c_{v,\mathrm{an}}(x,t)$ coupling term in Eq. (11) by its steady-state solution (Eq. (27)) (the time constant of the water vapor has been shown to be multiple orders of magnitude faster than that of the liquid water). Thus, for $s \geq s_{\mathrm{im}}$

$$\frac{\partial s}{\partial t} = \frac{\partial}{\partial x}\left(b_1 S^{b_2}\frac{\partial S}{\partial x}\right) + \frac{M_v \gamma}{\rho_l}(\alpha_1 e^{\beta x} + \alpha_2 e^{-\beta x}) \tag{33}$$

and for $0 < s < s_{\mathrm{im}}$

$$\frac{\partial s}{\partial t} = \frac{M_v \gamma}{\rho_l}(\alpha_1 e^{\beta x} + \alpha_2 e^{-\beta x}) \tag{34}$$

Figure 2 demonstrates that the steady-state solutions to the water PDEs lead to an exponential form for the vapor and a fractional power polynomial for the liquid. As shown in the figure, variation in the water vapor channel-side BC affects the liquid water distribution in addition to the obvious influence on the water vapor. When the channel water vapor is at saturation (dash-dot line in Fig. 2), the anode GDL-channel liquid water flow is high and flooding occurs. Lowering the channel water vapor to $c_v^{\mathrm{ch}*}$, the distributions change to the solid line and liquid accumulation stops because the GDL-channel liquid flow ceases. Continuous channel water vapor conditions below $c_v^{\mathrm{ch}*}$ result in the movement of the two-phase water (liquid and vapor) front from $x_{\mathrm{fr}}=L$ to an equilibrium point within the GDL $x_{\mathrm{fr}}<L$ (dashed line). Derivation, analysis, and discussion of the mobile front model and related mass transport claims are addressed in Ref. [8].

The lower subplot of Fig. 2 shows three different liquid water distributions. The three curves are close to each other because we picked a flooded operating condition very close to the balanced case. The proximity does not suggest, and should not be confused with, convergence.

4 Controllability/Observability

In Ref. [6], the six second-order PDEs describing reactant and water dynamics in both GDL are approximated by a coarse three-section spatial discretization of the GDL. The channel mass balance ordinary differential equations (ODEs) in each electrode are added to the GDL subsystem, leading to a 24-state nonlinear numeric model of ordinary differential-difference equations (full numeric model).

In the semi-analytic solutions (SAS), a combination of the quasi steady-state analytic solutions for the gas constituents $(c_{\mathrm{H}_2}(x), c_{\mathrm{O}_2}(x), c_{v,\mathrm{an}}(x), c_{v,\mathrm{ca}}(x))$ with the water saturation $(s(x,t))$ creates a numeric differential algebraic equation (DAE). Based on the model under consideration, a further reduction in the number of states is possible with the SAS. Since vapor only transport through the membrane is assumed, the modeled distribution of liquid water present in the cathode GDL does not influence the anode water distributions (as long as $s_{\mathrm{ca}} > 0$). We therefore propose both 11-state and 7-state reduced models.

A C/O analysis will determine whether it is mathematically possible to control the liquid water mass in the channel and hence, the GDL-channel BC to obtain Eq. (19), which is critical for the stabilization of the system. Linearization of both the numeric 24-state model and the reduced-order SAS models (11-state and 7-state), allows the generation of a state-space model form and use of C/O measures,

$$\dot{x} = Ax + Bu, \quad y = Cx + Du \tag{35}$$

The analysis is based upon a linearized system of switching nonlinear equations. Switching is introduced from Eq. (6) and can be seen explicitly in Eqs. (32) and (33) of the semi-analytic solution. The C/O anaylsis, and hence system linearization, will be considered for three scenarios: $s(L,t) < s_{\mathrm{im}}$ (receding front shown by dashed line in Fig. 2), $s(L,t) = s_{\mathrm{im}}$ (borderline nonflooding shown by solid line), and for net liquid flow into the channel (flooding with $s(L,t) > s_{\mathrm{im}}$, shown by the dash-dotted line).

4.1 Choice of Controllability-Observability Test. A number of C/O tests exist, ranging from the simple C/O matrix rank tests to computation of the respective Gramians to determine if they are positive definite. The application of C/O tests that depend upon the matrix rank evaluation proved to be unreliable for the model under consideration here due to the large condition number associated with the difference in mode speeds. Large condition numbers cause for concern, resulting in large differences in the singular values, which makes rank determination difficult.

In spite of the removal of the fast GDL gas states, the fast channel states remain, and thus the stiff system characteristics of our model lead to a large condition number. Unit scaling was performed to reduce the condition number but it can be shown that the minimum condition number (κ_{min}) is still on the order of 10^6.

The basic C/O matrix rank analysis tests using matrix rank tests will thus be avoided here due to their reliance on interpretation of the rank of matrices. A large condition number makes interpretation of rank subjective, as a decision must be made regarding C/O based on singular value relative magnitudes even though those values may on the order of 10^{30}. Further, the rank test does not provide information on which modes of the system are controllable/observable.

The Popov–Belevitch–Hautus (PBH) eigenvalue test has the benefit of being able to identify C/O for each mode because the controllability/observability test is applied for each eigenvalue/mode λ_i. The PBH eigenvalue method still requires rank determination of a matrix with a high condition number. The PBH eigenvector test, on the other hand, provides a simple means to associate modes and their relative controllability, yet does not require a matrix rank evaluation. The PBH eigenvector test is summarized from Ref. [15], let $\overline{q_i}$ be the ith LH (row) eigenvector of A associated with the λ_i eigenvalue $\overline{q_i}A = \lambda_i \overline{q_i}$, then define as $c_{\lambda_i} = |\overline{q_i}B|_2$. If c_{λ_i} is a small number, then λ_i is an uncontrollable state from the inputs that form the B matrix. Similarly, let $\overline{v_i}$ be the ith RH (column) eigenvector of A associated with the λ_i eigenvalue $A\overline{v_i} = \lambda_i \overline{v_i}$, then define as $o_{\lambda_i} = |C\overline{v_i}|_2$. If o_{λ_i} is a small number, then λ_i is an unobservable state from the outputs that form the C matrix.

The modes are tied to the physical states by inspection of the eigenvectors of the linearized system matrix A from Eq. (35). Most states are associated with only one eigenvalue (λ_i) and the corresponding eigenvector has only one significant nonzero element, hence identification of the corresponding state is straightforward. However, some system modes are coupled with several states and the c_{λ_i}s for these groupings are plotted together in Table 1. The o_{λ_i}s are listed in Table 2.

Table 1 Controllability PBH eigenvector test results

	Borderline			$0 < s_{an}[3] < s_{im}$			Flooding		
Mode	24	11	7	24	11	7	24	11	7
s^{GDL}_{an} (3 modes)	4.3e-5 ~ 1.0e-3	3.7e-5 ~ 7.9e-4	3.6e-4 ~ 7.6e-4	1.6e-4 ~ 9.1e-4	3.0e-4 ~ 7.9e-4	1.1e-4 ~ 8.0e-4	0	0	0
s^{GDL}_{ca} (3 modes)	7.5e-5 ~ 2.6e-3	1.4e-4 ~ 2.3e-3		4.3e-4 ~ 2.6e-3	1.1e-4 ~ 2.3e-3		0	0	
$m^{ch}_{w,ca}$	12.4	12.8		13.3	12.8		2.7E-03	2.5E-03	
$m^{ch}_{w,an}$	3.93	3.27	2.73	4.17	4.12	4.12	9.6E-04	8.3E-04	8.2E-04
c_{ca} (O_2, N_2 modes)	3.79 ~ 21.3	3.79 16.4	3.86 33.7	3.78 ~ 21.4	3.96 16.3	3.86 33.7	3.29 ~ 47.1	3.86 16.3	3.86 33.7
c_{H2}	7.85 ~ 9.87	7.76	7.71	3.98 ~ 10.5	7.75	7.74	9.8 ~ 19.2	19.4	19.4
($c_{v,e}$ @ mb)	**6.8E-04**			**6.9E-04**			0		
$c_{v,e}$ (6 modes)	**5.24 ~ 6.28**			**5.25 ~ 6.63**					

Table 2 Observability PBH eigenvector test results

	Borderline				$0 < s_{an}[3] < s_{im}$		Flooding				
Mode	24V	11V	11H	11VH	24V	11V	24V	11V	**11H**	11VH	7V
s^{GDL}_{an} (3 modes)	4.8e-3 ~ 5.4e-3	0	0	0	4.7e-3 ~ 7.4e-3	0	0.32 ~ 0.37	0.16 ~ 1.09	**0**	0.16 ~ 1.09	0.16 ~ 1.09
s^{GDL}_{ca} (3 modes)	4.0e-2 ~ 5.7e-2	0	0	0	9.8e-1 ~ 8.7e-2	0	0	0	**0**	0	
$m^{ch}_{w,ca}$	5.19	12.8	1.18	13.3	6.63	12.8	0	0	**0**	0	
$m^{ch}_{w,an}$	0.15	2.66	0.56	2.89	0.15	2.66	0.037	2.34	**0**	2.47	2.34
c_{ca} (O_2, N_2 modes)	3.73 ~ 15.1	8.50 18.1	0 0	8.50 18.1	3.73 ~ 15.1	8.50 18.1	2.63 ~ 15.3	8.50 18.1	**0** **0**	8.49 18.1	8.49 18.1
c_{H2}	0.09 ~ 0.30	0.46	0.23	0.46	0.09 ~ 0.38	0.46	0.09 ~ 0.37	0.49	**0**	0.49	0.46
($c_{v,e}$ @ mb)	**5E-09**				**8E-09**		**3e-10 ~ 7e-9**				
$c_{v,e}$ (6 modes)	**0.041 ~ 0.77**				**0.041 ~ 0.62**		**0.23 ~ 0.85**				

It is demonstrated that the degree of C/O is affected by the operating point. For example, with the inputs described in Sec. 4.2, greater controllability of the liquid water modes is obtained when the channel condition is subsaturated than when it is saturated. On the other hand, during anode flooding (which is associated with channel vapor saturation), though the GDL anode liquid water becomes uncontrollable, observability is gained using cell voltage output.

4.2 About Control Inputs and Outputs. The possible control inputs for our system are related to channel constituent flow rates. In practice, both anode and cathode inlet streams can be humidified, though it is typical in our experiments to set the cathode inlet at 100% and the anode inlet at nearly 0% relative humidity, respectively. For this study, the general case of actuation via variably humidified inlet stream is assumed for both electrodes, thus the relative humidity control inputs are set near the midpoint of their potential ranges (40–60%) during linearization. From a control standpoint, it is beneficial to keep actuators away from the saturation limits, 0% and 100%, so that they may be used effectively.

Typical implementation methods for the reactant flow rates include pressure control and flow control. In flow control, the upstream pressure is held constant and a valve opening position is determined to provide the desired flow rate into the channel

$$W^{\mathrm{in}} = u_{\mathrm{flow}} \cdot k^{\mathrm{in}}(p_{\mathrm{source}} - p^{\mathrm{ch}}) \tag{36}$$

where $u_{\mathrm{flow}} \in [0,1]$ is the position of the upstream valve, p^{ch} is the total pressure in the channel, p_{source} is the pressure upstream of the channel inlet, and k^{in} is an experimentally determined linear nozzle coefficient.

The flow in the channels can be related to reactant excess ratios λ_{H_2} and λ_{O_2}, which are important variables because they are used to assess the efficiency of the fuel cell through the reactant utilization. The controlled inputs that form the matrix B of the linear system are

$$u = [\mathrm{RH}^{\mathrm{in}}_{\mathrm{an}}, \mathrm{RH}^{\mathrm{in}}_{\mathrm{ca}}, u^{\mathrm{an}}_{\mathrm{flow}}, u^{\mathrm{ca}}_{\mathrm{flow}}] \tag{37}$$

In this work, 12 cases are studied combining variations in operating point and degree of model order reduction. Table 3 lists the key cases considered (each condition from column one is tested for each model of column two). The reduced state models are included in the analysis to confirm that the model reduction has not adversely affected the C/O. Additionally, for the 11-state model, four more tests combining the two practically available outputs were compared. The voltage output, based on a voltage model [6], and measurement of relative humidity (ϕ) in the channel were compared for flooding and borderline cases. The point is to determine the effect on observability for each of these outputs alone and together. The voltage model enables the greatest range of observable states, due to its dependence upon liquid water in the anode channel, concentrations of oxygen, hydrogen, water vapor at the membrane, stack current, and temperature (as shown in Ref. [6]),

$$v_{\mathrm{cell}} = f(m^{\mathrm{ch}}_{w,\mathrm{an}}, c^{\mathrm{mb}}_{v,\mathrm{an}}, c^{\mathrm{mb}}_{v,\mathrm{ca}}, c^{\mathrm{mb}}_{\mathrm{H}_2}, c^{\mathrm{mb}}_{\mathrm{O}_2}, i, T) \tag{38}$$

whereas relative humidity is only a function of water vapor concentration and temperature,

$$\phi = f(c^{\mathrm{ch}}_{v,\mathrm{an}}, T, P^{\mathrm{ch,an}}) \tag{39}$$

The total channel pressure $P^{\mathrm{ch,an}}$ is assumed to be constant.

Table 3 Controllability/observability cases studied

Condition	Model
Borderline	24-state full numeric model
$s[3] < s_{\mathrm{im}}$	11-state SAS model (6 GDL +4 channel states)
Flooding	7-state SAS model (3 GDL +4 channel states)

Table 4 Output matrix surrogate states

Removed state	Surrogate state
$c_{v,\mathrm{ca}}(x,t)$	$m^{\mathrm{ch}}_{w,\mathrm{ca}}$
$c_{v,\mathrm{an}}(x,t)$	$m^{\mathrm{ch}}_{w,\mathrm{an}}$
$c_{\mathrm{O}_2}(x,t)$	$c^{\mathrm{ch}}_{\mathrm{O}_2}$
$c_{\mathrm{H}_2}(x,t)$	$c^{\mathrm{ch}}_{\mathrm{H}_2}$

4.3 Surrogate States for Reduced Models. Residualization of the fast states by analytic solution to form algebraic equations has an influence on the state matrices of the fuel cell model. For example, in the full numeric 24-state model, the water vapor was a dynamic state in each spatially-discretized section. Upon implementation of the analytic solution for $c_{v,e}(x,t)$, the water vapor dynamic states are removed and the analytic solution is inserted into dynamic state equations for $s_{\mathrm{an}}(x,t)$. Given identical operating conditions, the SAS reduced model has very different state equations, as shown by Eqs. (40) and (41). Residualization of the fast states has transferred the contributions of the gas states in the full numeric model to the remaining dynamic states in the reduced-order model that determines their analytic solutions. These surrogate states are the boundary conditions for the analytic solutions implemented.

When reducing the full numeric system to a reduced-order system under nonflooding conditions, with $i = 0.25\ \mathrm{A\ cm}^{-2}$, $T = 333\ \mathrm{K}$, $\mathrm{RH}^{\mathrm{in}}_{\mathrm{an}} = 40\%$, $\lambda_{\mathrm{H}_2} = 285\%$, and voltage output, the linearized output matrix C is altered,

$$C_{\mathrm{full}} = 0.747 c_{v,\mathrm{an}}[1] + 0.747 c_{v,\mathrm{ca}}[1] + 0.493 c_{\mathrm{H}_2}[1] + 20.9 c_{\mathrm{O}_2}[1]$$

$$C_{\mathrm{red}} = 0.492 c^{\mathrm{ch}}_{\mathrm{H}_2} + 20.3 c^{\mathrm{ch}}_{\mathrm{O}_2} + 0.024 m^{\mathrm{ch}}_{w,\mathrm{an}} + 0.030 m^{\mathrm{ch}}_{w,\mathrm{an}} \tag{40}$$

Using as an example the liquid saturation nearest the channel, the state equations also change

$$\dot{s}_{\mathrm{an}}[3]_{\mathrm{full}} = 0.11 s_{\mathrm{an}}[2] - 0.13 s_{\mathrm{an}}[3] + 0.016 c_{v,\mathrm{an}}[3]$$

$$\dot{s}_{\mathrm{an}}[3]_{\mathrm{red}} = 0.08 s_{\mathrm{an}}[2] - 0.04 s_{\mathrm{an}}[3] + 0.02 m^{\mathrm{ch}}_{w,\mathrm{an}} \tag{41}$$

The hydrogen, oxygen, and anode vapor contributions have been related to their channel BC through the analytic solution and are represented by the associated channel states. The generation of water at the membrane and the humidification of the cathode inlet stream tends to lead to a condition of constant flooding and supersaturation in the cathode GDL. With the removal of the dynamic water vapor states, the cathode GDL water vapor distribution is influenced only through the membrane by the anode water vapor distribution. In the full numeric model, membrane water content is a function of the humidities in both anode and cathode at $x = 0$. However, with the removal of water vapor states, Table 4 shows that the water vapor concentration membrane gradient becomes only a function of channel water vapors. Thus, if a channel water vapor condition becomes saturated, it is no longer a dynamic state, with that state's impact on the input/output relegated to changes in $c^{\mathrm{sat}}_{v}(T_{\mathrm{st}})$.

4.4 Controllability/Observability Results. The results of the C/O analysis achieved by varying the subsaturated anode inlet gas feed rate for an operating condition near the borderline case between flooding and receding liquid water distributions in the anode GDL of a PEMFC is presented. Although the linearization results presented in this work consider only one operating current density and temperature, both of which have a strong nonlinear influence on the model, by considering the three cases (flooding, borderline, and receding) the major switching nonlinearity in the model is examined, which impacts the C/O results. Varying temperature and current density will impact the control inputs (u) and state equilibrium point (x) at which the borderline case exists and perhaps the existence of that equilibrium for reasonable inputs.

Of foremost concern is that all the unstable modes are controllable and observable. In Ref. [14], it was shown that the liquid water states within the GDL are stable under any reasonable range of conditions if the channel water mass state is bounded yet the channel liquid water mass can experience unbounded growth from bounded inputs. This anode channel instability leads to voltage degradation in the short term and will cause fuel cell shut down if not addressed.

The results of the PBH eigenvector tests for the various model cases and condition sets are shown in Tables 1 and 2. In the table headings, the number refers to the number of states in the model (24 is the full numeric model). The letter (in the observability table) indicates the output used (voltage and/or humidity of the anode channel). The modes column references mode groupings of states. Due to the nature of the difference-equation generated modes and the model, states of the same class (H_2 concentration ($c_{H_2}^{GDL}$), anode GDL liquid water (s_{an}^{GDL}), etc.) tend to form modes together. Because the liquid vapor modes could not be separated within an electrode GDL or even across the membrane due to the membrane transport model, all water vapor concentration modes have been lumped into $c_{v,e}$.

The C/O tests for the various cases result in the following conclusions (from data shown in Tables 1 and 2).

1. Under flooding conditions (nonzero liquid water in the channel), the masses of water in the channels are controllable modes and can thus be steered back to zero with the system inputs (shaded cells in Table 1).
2. The GDL liquid water modes ($s_{an}^{GDL}, s_{ca}^{GDL}$) are controllable under all nonflooding conditions (Table 1).
3. During flooding, the water vapor ($c_{v,e}$) and liquid water modes in the GDL are uncontrollable. Small changes in anode inlet/outlet flow characteristics do not influence water vapor concentration in the channel because of the model assumption that super-saturation is not obtainable, thus until the channel liquid water is removed; influence on GDL water states is effectively blocked.
4. Under nonflooding conditions, the connection (Eqs. (1) and (3)) between water vapor and liquid water in the 24-state models enables weak observability through the water vapor presence in the voltage model. This observability is lost in the reduced-order models because the weak link between vapor diffusivity and liquid water was eliminated to obtain the analytic solution of the water vapor concentration PDE.
5. With cell voltage as an output, observability of anode liquid water improves with flooding conditions as the liquid water is seen in the degradation of the voltage [4] due to liquid buildup (shaded cells of Table 2).
6. The number of observable modes increases significantly with use of voltage output versus the use of relative humidity alone due to the many states contributing to the voltage estimation.
7. Use of relative humidity output alone results in unobservability for all system modes during flooding (Flooding 11H case, Table 2).
8. Combination of both outputs does not increase the number of modes that are observable due to output state redundancy; however, observability of the channel water modes improves when both outputs are used (dash-dot border cells in Table 2).
9. A deficiency in the model is suggested by the controllability/observability results for the water vapor concentrations at the membrane. A water vapor mode with an equal influence from both anode and cathode sections nearest the membrane is both extremely fast and has very low controllability (four orders of magnitude less than the other GDL water vapor modes. This inconsistency is expected to be directly to the lack of dynamics in the membrane water transport model (double-line border in Tables 1 and 2).

The significance of the above results can be summarized.

1. Though GDL liquid modes are not controllable under flooding, stabilization of the anode water dynamics is possible since the unstable anode channel water mass is controllable.
2. The unobservable anode channel water mass when ϕ is the only output during flooding implies that though the water mass can be driven to zero, the controller will not have any information on when the mass will be eliminated. If integral control is used, wind-up will be a concern. A combination of cell voltage and relative humidity outputs would alleviate this issue by making the water mass observable. Each of these two outputs provides important information lacking in the other; voltage output informs the controller that actuation is needed and ϕ has information regarding whether drying or flooding is causing the voltage loss.
3. Together with channel liquid controllability above, controllability of the GDL liquid modes under all nonflooding conditions implies that the GDL liquid distribution can be shaped by the proposed inputs.
4. As the GDL liquid state $s[3]$ nearest the channel falls below the immobile saturation, controllability of liquid modes is essentially unchanged, providing evidence that the system "switch" from nonzero to zero liquid flow into the channel will not be an issue for control around the desired setpoint.

5 Conclusions

The C/O analysis applied to the reduced and full order unit fuel cell models of liquid water transport within the anode GDL of a PEMFC indicates that the liquid distribution within the GDL is controllable during nonflooding channel conditions, implying that practical fuel cell inputs can be effectively used to prevent anode flooding. Further, the channel water mass is controllable even under flooding conditions. Under flooding conditions, the combination of voltage and channel humidity outputs renders the channel water mass observable, thus state feedback to stabilize the channel water is feasible. Use of channel humidity as the sole output is of questionable value as the channel water mass is not observable during flooding conditions.

Acknowledgment

Funding is provided from NSF-GOALI (Contract No. CMS-0625610) and TEMA.

Table 5 Inputs used for linearization

Condition	λ_{H_2}	I_{st} (A)	λ_{O_2}	Temperature (K)	RH_{an} (%)	RH_{ca} (%)
Borderline	2.85	75	3.0	333	40	50
Flooding	2.50	75	3.0	333	40	50
Receding	2.90	75	3.0	333	40	50

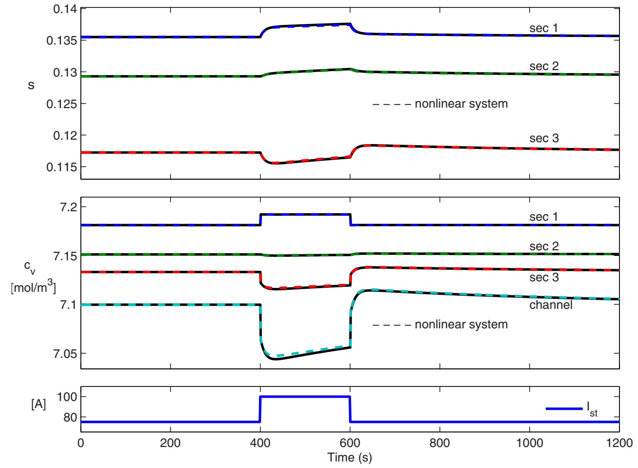

Fig. 3 Borderline case: linear system tracks nonlinear system for a stack current step up/down of 25 A

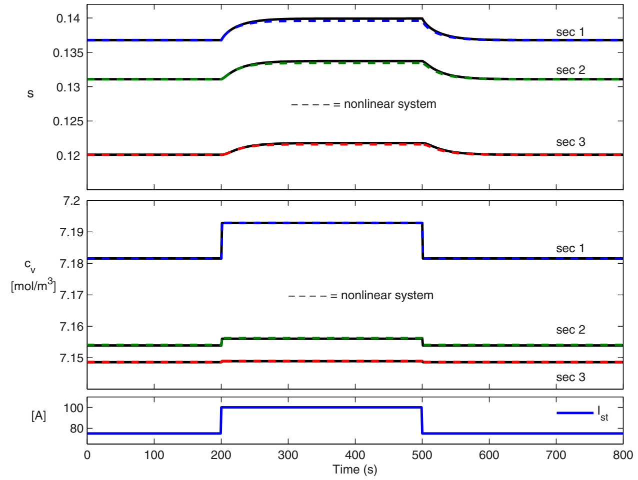

Fig. 4 Flooding case: linear system tracks nonlinear system for a stack current step up/down of 25 A

Appendix

Examples show that the linearized 24-state model accurately reflects the nonlinear system response to small input variations from equilibrium. Table 5 lists the key equilibrium values. In order to obtain linearization models, only the hydrogen stoichiometry was varied due to its strong influence on anode channel water mass (i.e., water vapor concentration). The fuel cell active area used for simulation is 300 cm^2, therefore a stack current of I_{st} $=75$ A, corresponds to current density $i=0.25$ A cm^{-2}.

In this application, a coarse spatial discretization of the GDL into three sections was performed. Section 1 is closest to the membrane for anode and cathode and section 3 is next to the channel.

The top subplots of Figs. 3 and 4 show s, the time-varying water saturation, for applicable sections of the GDL (typical values are between 0.11 and 0.16). The middle subplots show the water vapor concentration for the channel and each section.

Finally, the bottom subplots show the stepped input stack current. With changes in I_{st}, both s and c_v respond due to the dependence of anode flow rate and water production on stack current. For borderline and drying (not shown) cases, the inverse relationship between stack current and channel vapor concentration can be explained by the increase in subsaturated inlet gas flow rate, due to the operation with a constant stoichiometric flow. The vapor concentration in the GDL, sections 1–3, each responds to the change in boundary condition to a lesser degree. The response of liquid water saturation in the section near the channel also shows an inverse response to the increase in I_{st} since the vapor concentration of that section is driven below the saturation value, hence evaporating liquid from that region, while sections near the membrane move increasingly with I_{st} due to the higher water crossover rate. However, under the flooding case, all sections are positively correlated with I_{st}. As can be seen from Figs. 3 and 4, the linearizations match the nonlinear system responses well for I_{st} steps up/down. Though not shown here, significantly larger input steps than those of Figs. 3 and 4 will result in notable response error (i.e., effect of nonlinearities).

References

[1] Pasaogullari, U., and Wang, C.-Y., 2005, "Two-Phase Modeling and Flooding Prediction of Polymer Electrolyte Fuel Cells," J. Electrochem. Soc., **152**(2), pp. A380–A390.

[2] Zhang, F. Y., Yang, X. G., and Wang, C. Y., 2006, "Liquid Water Removal From a Polymer Electrolyte Fuel Cell," J. Electrochem. Soc., **153**(2), pp. A225–A232.

[3] Siegel, J. B., McKay, D. A., Stefanopoulou, A. G., Hussey, D. S., and Jacobson, D. L., 2008, "Measurement of Liquid Water Accumulation in a PEMFC With Dead-Ended Anode," J. Electrochem. Soc., **155**(11), pp. B1168–B1178.

[4] Pasaogullari, U., and Wang, C.-Y., 2004, "Two-Phase Transport and the Role of Micro-Porous Layer in Polymer Electrolyte Fuel Cells," Electrochim. Acta, **49**(25), pp. 4359–4369.

[5] Kumbur, E., Sharp, K., and Mench, M., 2006, "Liquid Droplet Behavior and Instability in a Polymer Electrolyte Fuel Cell Flow Channel," J. Power Sources, **161**(1), pp. 333–345.

[6] McKay, D. A., Siegel, J. B., Ott, W., and Stefanopoulou, A. G., 2008, "Parameterization and Prediction of Temporal Fuel Cell Voltage Behavior During Flooding and Drying Conditions," J. Power Sources, **178**(1), pp. 207–222.

[7] McCain, B. A., Stefanopoulou, A. G., and Kolmanovsky, I. V., 2007, "A Multi-Component Spatially-Distributed Model of Two-Phase Flow for Estimation and Control of Fuel Cell Water Dynamics," Proceedings of the 46th IEEE Conference on Decision and Control, pp. 584–589.

[8] McCain, B., Stefanopoulou, A., and Kolmanovsky, I., 2009, "A Dynamic Semi-Analytic Channel-to-Channel Model of Two-Phase Water Distribution for a Unit Fuel Cell," IEEE Trans. Control Syst. Technol., **17**(5), pp. 1055–1068.

[9] Nam, J., and Kaviany, M., 2003, "Effective Diffusivity and Water-Saturation Distribution in Single and Two-Layer PEMFC Diffusion Medium," Int. J. Heat Mass Transfer, **46**, pp. 4595–4611.

[10] Kumbur, E., Sharp, K., and Mench, M., 2007, "On the Effectiveness of Leverett Approach for Describing the Water Transport in Fuel Cell Diffusion Media," J. Power Sources, **168**(2), pp. 356–368.

[11] Wang, X., and Nguyen, T. V., 2008, "Modeling the Effects of Capillary Property of Porous Media on the Performance of the Cathode of a PEMFC," J. Electrochem. Soc., **155**(11), pp. B1085–B1092.

[12] Sinha, P., and Wang, C.-Y., 2007, "Pore-Network Modeling of Liquid Water Transport in Gas Diffusion Layer of a Polymer Electrolyte Fuel Cell," Electrochim. Acta, **52**, pp. 7936–7945.

[13] Gan, M., and Chen, L.-D., 2006, "Analytic Solution for Two-Phase Flow in PEMFC Gas Diffusion Layer," ASME Fuel Cell 2006.

[14] McCain, B. A., Stefanopoulou, A. G., and Kolmanovsky, I. V., 2008, "On the Dynamics and Control of Through-Plane Water Distributions in PEM Fuel Cells," Chem. Eng. Sci., **63**(17), pp. 4418–4432.

[15] Kailath, T., 1980, *Linear Systems*, 1st ed., Prentice-Hall, Englewood Cliffs, NJ.